Microfluidic analysis of cellular deformability of normal and oxidatively damaged red blood cells

Joanne M. Kwan,[1,2] Quan Guo,[3] Dana L. Kyluik-Price,[1,2] Hongshen Ma,[1,3] and Mark D. Scott [1,2,4]*

Microfluidic analysis of blood has potential clinical value for determining normal and abnormal erythrocyte deformability. To determine if a microfluidic device could reliably measure intra- and inter-personal variations of normal and oxidized human red blood cell (RBC), venous blood samples were collected from repeat donors over time. RBC deformability was defined by the cortical tension (pN/μm), as determined from the threshold pressure required to deform RBC through 2–2.5 μm funnel-shaped constrictions. Oxidized RBC were prepared by treatment with phenazine methosulphate (PMS; 50 μM). Analysis of the control and oxidized RBC demonstrated that the microfluidic device could clearly differentiate between normal and mildly oxidized (20.13 ± 1.47 versus 27.51 ± 3.64 pN/μm) RBC. *In vivo* murine studies further established that the PMS-mediated loss of deformability correlated with premature clearance. Deformability variation within an individual over three independent samplings (over 21 days) demonstrated minimal changes in the mean pN/μm. Moreover, inter-individual variation in mean control RBC deformability was similarly small (range: 19.37–21.40 pN/μm). In contrast, PMS-oxidized cells demonstrated a greater inter-individual range (range: 25.97–29.90 pN/μm) reflecting the differential oxidant sensitivity of an individual's RBC. Importantly, similar deformability profiles (mean and distribution width; 20.49 ± 1.67 pN/μm) were obtained from whole blood via finger prick sampling. These studies demonstrated that a low cost microfluidic device could be used to reproducibly discriminate between normal and oxidized RBC. Advanced microfluidic devices could be of clinical value in analyzing populations for hemoglobinopathies or in evaluating donor RBC products post-storage to assess transfusion suitability. Am. J. Hematol. 88:682–689, 2013. © 2013 Wiley Periodicals, Inc.

Introduction

The biconcave, anuclear, human red blood cell (RBC) circulates for approximately 120 days delivering oxygen to, and removing carbon dioxide from, tissues and organ. To accomplish these functions, the approximately 8 μm diameter RBC must traverse capillaries that are as small as 2–2.5 μm in diameter and splenic interendothelial clefts that are only 0.5–1.0 μm in diameter [1–5]. Successful transit of these anatomical structures is dependent upon the deformability of the RBC. Cellular deformability is a function of its surface to volume ratio, cytoplasmic viscosity, and membrane viscoelasticity [6–10]. Biological, pharmacological or biochemical changes that affect any of these variables can contribute to loss of cellular deformability and the premature clearance of the RBC via capillary or splenic sequestration, phagocytosis or intravascular lysis [3,11–16]. If sufficient RBC are lost, anemia and tissue hypoxia will result. Hence, normal RBC deformability is crucial for circulatory efficiency and biological viability.

Altered cellular deformability is a component of multiple clinically significant red cell abnormalities and hemoglobinopathies such as Sickle Cell Disease (SCD) or β-Thalassemia [3,16–23]. In SCD, the inter-chain hydrophobic interactions and polymerization of the deoxygenated hemoglobin impairs deformability as well as promotes microocclusions via vasculature adhesion and blockage [18]. In β-Thalassemia, the unpaired and unstable α-hemoglobin chains generate reactive oxygen species damaging cytoskeletal proteins and oxidizing lipids and also tightly adhere to the membrane leading to a reduction in cellular deformability. The loss of deformability is further compounded by the decreased surface area to volume ratio of the microcytic red cells [3,17,22]. Experimentally, the aforementioned red cell damage can be modeled by exposing them to oxidants such as phenazine methosulphate (PMS) [3,15,17,24,25].

To understand the pathophysiology of disease, previous investigators have used techniques such as ektacytometry and the cell transit analyzer to measure cellular deformability [3,26–33]. Ektacytometry measures deformability by subjecting RBC suspended in a viscous solution to rotational shear stress such that the normal cells form ellipsoids. The extent of ellipsoid formation is dependent the on deformability of the cell with non-deformable cells showing minimal shape change. The scatter intensity pattern from laser diffraction produces isointensity curves and deformability indices. This method only indicates the average deformability of a cell population and cannot accurately and efficiently quantify the amount of rigid cells in a bimodal population where both normal and abnormal cells are present [26,32]. In the cell transit analyzer, itself a microfluidic device, a cell passes through a micropore of fixed diameter and length with electrical resistance

[1]Centre for Blood Research, University of British Columbia, Vancouver, British Columbia, Canada; [2]Department of Pathology and Laboratory Medicine, University of British Columbia, Vancouver, British Columbia, Canada; [3]Department of Mechanical Engineering, University of British Columbia, Vancouver, British Columbia, Canada; [4]Canadian Blood Services, University of British Columbia, Vancouver, British Columbia, Canada

Conflict of interest: Nothing to report

*Correspondence to: Mark D. Scott, Canadian Blood Services and the Centre for Blood Research, University of British Columbia, Life Sciences Centre, 2350 Health Sciences Mall, Vancouver, BC V6T 1Z3, Canada. E-mail: mdscott@mail.ubc.ca

Contract grant sponsors: Canadian Institutes of Health Research (CIHR), Canadian Blood Services (CBS), and Health Canada.

Received for publication 21 February 2013; Revised 24 April 2013; Accepted 30 April 2013

Am. J. Hematol. 88:682–689, 2013.

Published online 14 May 2013 in Wiley Online Library (wileyonlinelibrary.com).
DOI: 10.1002/ajh.23476

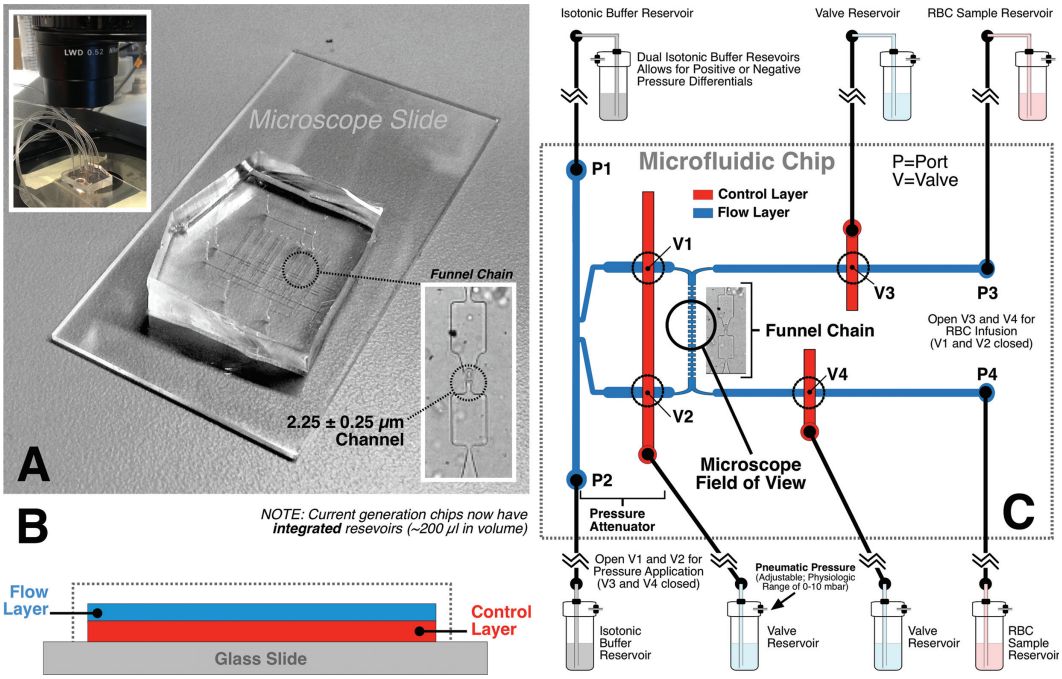

Figure 1. Panel A: Shown is a photograph of the microfluidics device with a magnification of the funnel chain depicting an erythrocyte transiting through the microfluidic pore. The geometry of the pore was approximately 2–2.5 μm wide with a height of 3.15 μm. Panel B; Shown is the layer construction of the microfluidic device. Panel C: A schematic design of the microfluidic device is illustrated. Valves 1–4 mark the intersection of the control and flow layers, and can be opened and closed to control fluid movement within the flow layer. As a result of the precisely controlled fluid movement, test cells transit through the pores of the funnel chain, have their threshold pressure measurements recorded, and exit through the Waste Outlet.

generated by a conductometer. The surrounding fluid creates a pressure gradient which forces a cell through the micropore and its resistive pulse is measured and transformed into useful measurements such as transit time. However, the sensitivity of this method may vary with cell size (smaller cells pass through with less resistance) and RBC concentration in suspension. The abnormally large or rigid cells, which are clinically important, would also block the micropore and be excluded from analysis [3,28,34]. Moreover, these traditional deformability assays are relatively large devices that require expensive instrumentation and are labor-intensive and time-consuming procedures that are ill-suited for rapidly screening donor blood prior to transfusion or for screening individuals (or entire villages) for the red cell abnormalities such as SCD or thalassemias.

A potentially promising, cost-effective, and high throughput method for measuring RBC deformability is microfluidics [35–41]. Deformability measurements using microfluidics uses minute amounts of a whole blood or RBC suspension flowing through a funnel-shaped microconstriction [42–44]. The threshold pressure required for a sample of RBC to traverse the defined constriction is determined and converted to a quantitative measure (cortical tension; pN/μm) of cellular deformability. Importantly, these microfluidic measurements provide both individual RBC and populational assessments of cellular deformability. Additional advantages of microfluidics analysis include the requirement for small sample volumes, low-cost, and high resolution and sensitivity [35]. To experimentally test a prototype microfluidic RBC deformability device, normal and oxidatively damaged RBC were measured in a small sample of blood donors over several weeks [43,44]. As demonstrated in this study, microfluidics provided reproducible intra- and inter-individual data and demonstrated its utility in detecting oxidatively damaged RBC.

Materials and methods

RBC preparation and treatment

Following informed consent, whole blood was collected from normal donors ($N = 19$) for microfluidic deformability analysis. From these donors, four individuals were selected for repeat venous whole blood sampling (Sodium heparin Vacutainer® collection tubes; BD, Franklin Lakes, NJ) over a period of up to 21 days. All other donors were sampled via finger pricks with the blood collected immediately in phosphate buffered saline (PBS; pH 7.4) for microfluidic analysis. For the four repeat donors, whole blood was centrifuged at 1000 × g for 5 minutes using Clay Adams Serofuge in order to remove the plasma, platelets, and white blood cells and washed (3x) in isotonic saline. The hematocrit of the packed RBC was assessed and the washed RBC were resuspended to a 20% hematocrit in Hank's Balanced Salt Solution (HBSS; 5 mM glucose and without $CaCl_2$ and $MgSO_4$; Invitrogen by Life Technologies, Carlsbad, CA). An aliquot of the 20% hematocrit RBC stock was treated with 50 μM phenozine methosulfate (PMS; Sigma-Aldrich, St. Louis, MO) for 60 minutes at 37°C to mildly oxidize the cells [15,24]. Sham-treated (0 μM PMS) control cells were similarly incubated. Following incubation, the samples were centrifuged (1000 × g for 5 minutes) and washed twice with isotonic saline. Upon the final wash, the control and oxidized RBC were resuspended to a 40% hematocrit in HBSS-containing penicillin/streptomycin for subsequent microfluidic deformability analysis. Aliquots of the control and oxidized RBC samples were analyzed in parallel using a Siemens Advia 120 Hematology System (Siemens, Mississauga, Canada).

RBC morphology

Samples from the venous blood donors were assessed for morphology via microscopic analysis. At each sampling point, control and PMS-oxidized sample aliquots were examined for morphology. RBC samples were fixed using paraformaldehyde immediately post-treatment (sham or PMS). Multiple random fields were selected and photomicrographs were taken using a Zeiss Axioplan 2 (Micro-Optik, Deursen, Netherlands) or Olympus CK40 (Olympus America, Melville NY, USA) microscope at 100x magnification.

Murine transfusion model

To correlate the effects of PMS-oxidation on *in vitro* deformability with *in vivo* survival, murine transfusion studies were done. Whole

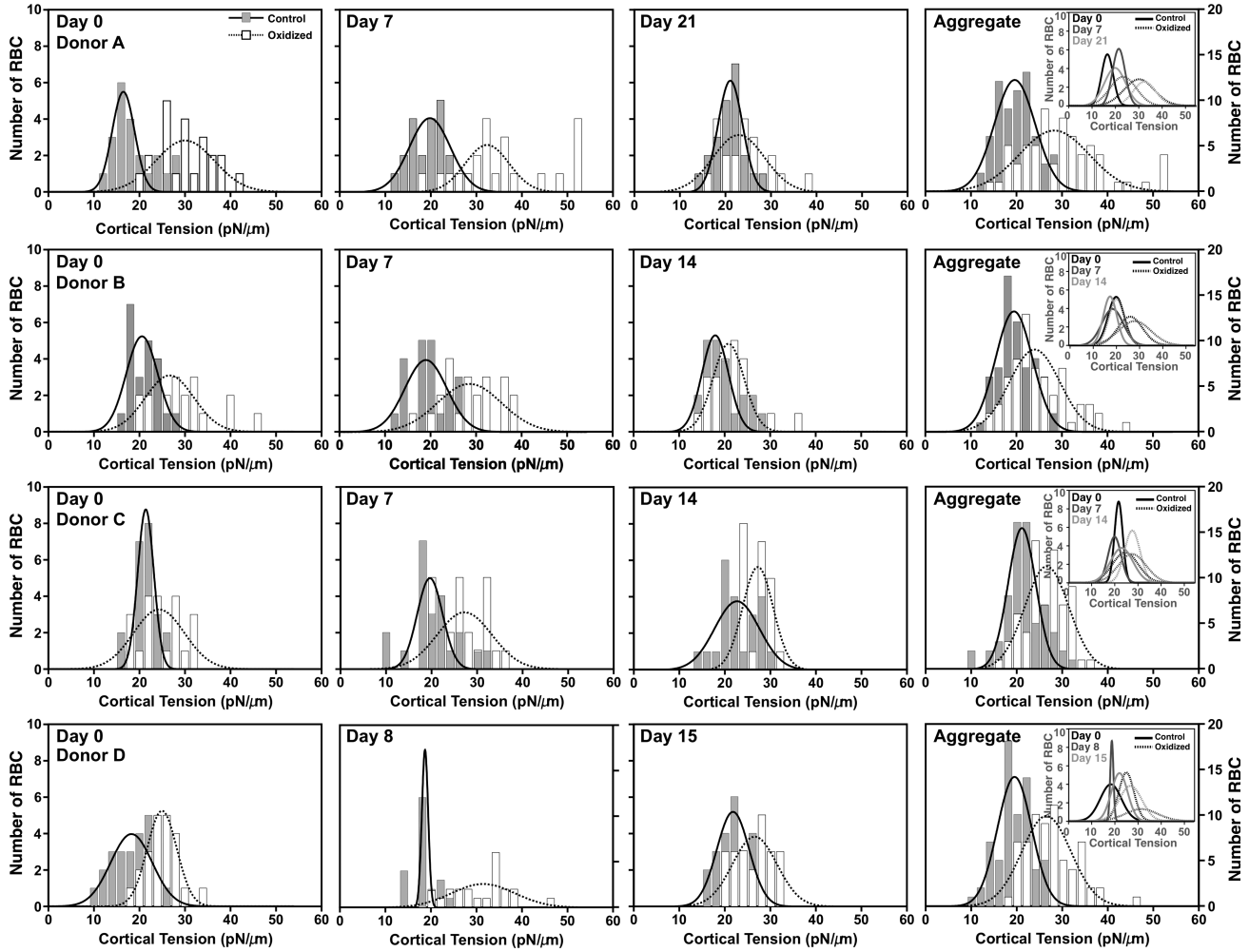

Figure 2. Cellular deformability profiles of control and PMS-oxidized RBC show a significant ($P < 0.001$) separation in mean cortical tension and cell distribution width on both an intra- and inter-individual basis. As shown, three independent sampling of four individuals over several days (0–21 days) demonstrated an ability to detect the rigid oxidized sample from the untreated control cells based on both the mean cortical tension and the cell distribution width. The aggregate profile was averaged from the three independent sample points. Shown as INSERTS within each aggregate profile are the overlapped distribution curves for the control and oxidized RBC shown in the leftward panels. This data demonstrates the reproducibility of the prototype micofluidic device.

blood was obtained from donor mice (Balb/c) and washed (3x) in isotonic saline. As per the human samples, murine RBC was sham or PMS treated. The control and oxidized RBC were analyzed via the microfluidic device to obtain deformability profiles. For the *in vivo* survival studies, murine RBC were labeled using a fluorescent, membrane anchored marker, PKH-26 (Sigma, St. Louis, MO) [45,46]. Equal numbers of control or oxidized RBC (40% hematocrit) were transfused as previously described [46,47]. Blood samples from the recipient mice were followed until the labeled RBC were cleared from circulation (approximately 40–50 days for allotransfusions). Survival of fluorescently labeled control and PMS-oxidized RBC was monitored by analyzing the percent of fluorescently labeled RBC by flow cytometry (FACSCalibur Flow Cytometer, BD Biosciences, San Jose, CA) [45,46]. To better correlate PMS-treatment with a known hematological abnormality, model murine ß thalassemic cells were prepared via osmotic lysis and resealing as previously described [3,17,48,49]. Model ß thalassemic murine RBC are produced via the entrapment of purified human alpha-hemoglobin chains within normal murine RBC. Human model ß-thalassemic cells have previously been shown to exhibit structural and function changes very similar to patient derived samples [3,17,49]. The model murine ß thalassemic cells were labeled with PKH-26 and *in vivo* survival was followed as above.

Microfluidic fabrication

Microfluidic devices were fabricated using standard techniques of photolithography and multilayer soft lithography. Silicon master molds were initially fabricated using photolithography and the master molds were then replicated on demand using Polydimethylsiloxane (PDMS) via multilayer soft lithography technique as previously described [43,44]. Two molds (noted as control and flow layer molds) were used to fabricate the device out of PDMS (Fig. 1B). The design of the two-layer microfluidic device is shown in Fig. 1. The intersection of the two layer creates a thin membrane and by pressurizing fluid through the control layer, the membrane deflects and forms a temporary seal on the upper flow channel. The thickness of the flow layer channel on the mold was approximately 3.15 μm to allow the RBC to transit through without folding up. The thickness of the control layer channel molds was approximately 25 μm. The permanent bonding of the two layers, as well the bonding of the entire device to the glass slide, were carried out through air plasma bonding using plasma generator (Model PDC-001; Harrick Plasma, Ithaca, NY). These on-chip valves functionally separate the device into two parts: cell introduction and pressure attenuation. A diluted red cell suspension is introduced through inlet at port 3 (P3) with valve 1 and 2 shut. As a single cell is infused into the funnel chain area, valves 1 and 2 are opened while valves 3 and 4 are shut. This configuration allows the attenuated form of the pressure to be applied across the funnel chain. Pneumatic pressure is applied to the device (0.3 mbar resolution, range: 1–1000 mbar). The differential pressure is used to move the cell to the desired funnel location and to measure the threshold pressure required to deform a single cell through the funnel pore constriction. The funnel chain is composed of a series of funnels with decreasing pore sizes. The width of the funnel shaped micropore constriction used to measure RBC deformability was approximately 2 – 2.5 μm in size at its minimum.

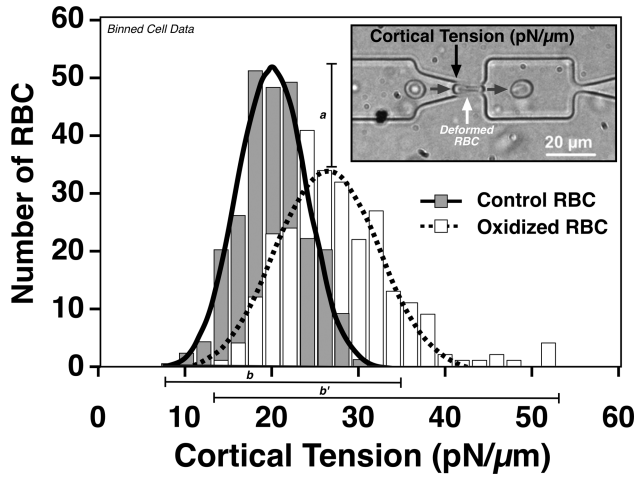

Figure 3. Population analysis of normal and PMS-oxidized RBC demonstrated a clear loss of deformability upon oxidation as shown by a significant ($P < 0.001$) increase in mean cortical tension. As shown, the mean cortical tension of normal and PMS-oxidized RBC was 20.13 ± 1.47 and 27.51 ± 3.64 pN/μm, respectively. The narrower distribution width of the normal RBC relative to the oxidized cells is reflected by the decreased peak height (*a*) of the cell count. Moreover, the extended distribution width and tail of the oxidized RBC (*b'*) relative to the control cells (*b*) was of diagnostic importance. The data shown is the summation of 12 control and 12 oxidized RBC samples from four individuals. INSERT: Shown is a photomicrograph of an RBC transiting the funnel constriction in the microfluidic channel.

Microfluidic deformability measurements

For each sampling point, both control and oxidized RBC were analyzed on the microfluidic device. Prior to testing, the flow channels were filled with 3 mL PBS (50 mM dibasic potassium phosphate, 105 mM NaCl, pH 7.4) and 5% bovine serum albumin (BSA; Sigma-Aldrich, St. Louis, MO) for 30 minutes to remove air bubbles and prevent non-specific cell interactions with the surface. The control channels were filled with de-ionized water. A suspension containing 10 μL of the 40% hematocrit sample in 3 mL of PBS with 5% BSA was made in 15 mL conical tubes with a customized sealed cap to feed the suspension into the cell inlet via Cole-Parmer 0.5 mm ID flexible Tygon tubing (Fisher Scientific, Ottawa, ON). Valves 1 and 2 (Fig. 1C) were closed while Valves 3 and 4 were kept open as the test cells migrated towards the funnel chain. When a single test cell reached the entrance of the funnel chain, the state of the valves was reversed (Valves 1 and 2 activated while Valves 3 and 4 closed). The precise and attenuated pressure (from pressure applied across port 1 and 2 via pressure attenuator) with resolution of ~0.3 Pa (Pascal) was used to determine the threshold pressure required to squeeze a single RBC through the last funnel with minimum constriction (pore size) ranging from 2 to 2.5 μm. Some variation in pore size was noted due to the fabrication process. The microfluidic deformability analysis initially used a relatively low pressure (~3 Pa after attenuation) to move the RBC to the mouth of the funnel. Once a cell arrived at the funnel, pressure was then gradually increased until a small portion of cell protruded through the funnel (Fig. 1). The cell would subsequently eject through the funnel pore rapidly. The threshold pressure (Eq. (1)) required to induce the RBC transit was then recorded for the determination of cortical tension. Typically 25–30 cells were tested per sample per device.

Data analysis

The *Law of Laplace* was used to convert the pressure measurements to cortical tension using Eq. (1) in order to correct for the variation of red cell sizes as well as funnel pore geometries [43,44]. Although the *Law of Laplace* model has been traditionally applied to micropipette aspiration where a part of the cell membrane is suctioned into a circular orifice, this model makes no assumptions about the geometry of the orifice. The only requirement is a uniform surface tension and the membrane forms an effective seal at the constriction. Since both of these assumptions seem reasonable based on evaluation of the deformation process, we believed this model was appropriate phenomenological representation of cell deformability to account for variations in constriction size and cell size.

TABLE I. Advia Hematology Analyzer Findings on Normal and Oxidized Donor RB

	Normal range	Untreated RBC mean ± SD	Oxidized RBC mean ± SD
RBC ($\times 10^{12}$ cells/L)	3.8–5.8	4.02 ± 0.08	3.97 ± 0.06
HGB (g/L)	115–175	123.58 ± 2.89	122.42 ± 1.10
HCT (L/L)	0.35–0.50	0.37 ± 0.00	0.38 ± 0.01
MCV (fL)	82–98	92.96 ± 1.43	94.69 ± 1.49
MCH (pg)	28–34	30.79 ± 0.56	30.82 ± 0.40
MCHC (g/L)	320–365	331.33 ± 3.97	325.67 ± 2.62*
CHCM (g/L)	330–370	330.83 ± 2.41	320.67 ± 3.37[a]*
CH (pg)	–	30.60 ± 0.31	30.21 ± 0.34
RDW (%)	11–15	13.42 ± 0.63	13.26 ± 0.65
HDW (g/L)	22–32	23.40 ± 1.93	22.98 ± 2.01

$N \geq 16$ per condition.
[a] Out of reference range.
*$P < 0.05$.

$$\Delta P = T_c\left(\frac{1}{R_a} - \frac{1}{R_b}\right) \quad (1)$$

As shown, T_c is the cortical tension in the cell membrane, R_a and R_b are the radius of curvature of the leading and trailing cell surface in the funnel constriction. At the critical moment when the cell transits through the funnel constriction where ΔP is the threshold pressure, R_a is assumed to be one half of the width of constriction and R_b is determined from the geometry of the funnel and the cell using volume conservation. The diameter of each RBC was measured optically in the microchannel where the discoid cell was rotationally constrained to be parallel with the focal plane of the microscope by the channel geometry. The volume was then estimated by the measured diameter of the cell with a fixed thickness of 2.5 μm. Data from each experiment were then binned into discreet cortical tension blocks of 2 pN/μm size to generate histograms and normal distribution profiles using Graphpad Prism. For statistical analysis, paired sample *t*-tests were performed to determine the significance between control and oxidized treatment groups on an intra- and inter-individual basis. A minimum *P*-value of ≤ 0.05 was used to determine significance.

Results

To determine the utility and reproducibility of a microfluidic device to measure the deformability of normal and PMS-oxidized RBC, donor cells from four healthy individuals were sampled three times over a period of up to 21 days. Analysis of the control and oxidized samples demonstrated that the prototype microfluidic device could clearly differentiate between the normal and oxidized RBC at all sampling points. The data, summarized in Fig. 2, demonstrated both intra-individual and inter-individual reproducibility of the microfluidic assay. Analysis of the data demonstrated that the mean ± SD of the normal, washed, RBC for Donors A–D were: 19.83 ± 0.95, 19.90 ± 1.04, 21.40 ± 1.61, and 19.37 ± 1.94 pN/μm, respectively (no significant difference between individuals; $P > 0.05$ for all samples). Importantly, the microfluidic devices were also highly capable of detecting deformability changes arising from mild oxidation of the donor cells. As shown in Fig. 2, the mean ± SD of the PMS-oxidized RBC for Donors A–D were: 29.90 ± 6.21, 26.83 ± 3.15, 25.97 ± 1.45, and 27.33 ± 3.06 pN/μm, respectively. Moreover, as shown by Fig. 2, normal RBC tended to have a smaller populational distribution width relative to the oxidized/abnormal RBC, where the distribution width parameter is somewhat analogous to the Red Cell Distribution Width (RDW) obtained using automated hematology analyzers. However, some of the variation in the curve distribution between the sample dates likely arose due to slight variations in the manufacturing tolerances of the prototype microfluidic device and due to biological variation (e.g., hydration) within an individual.

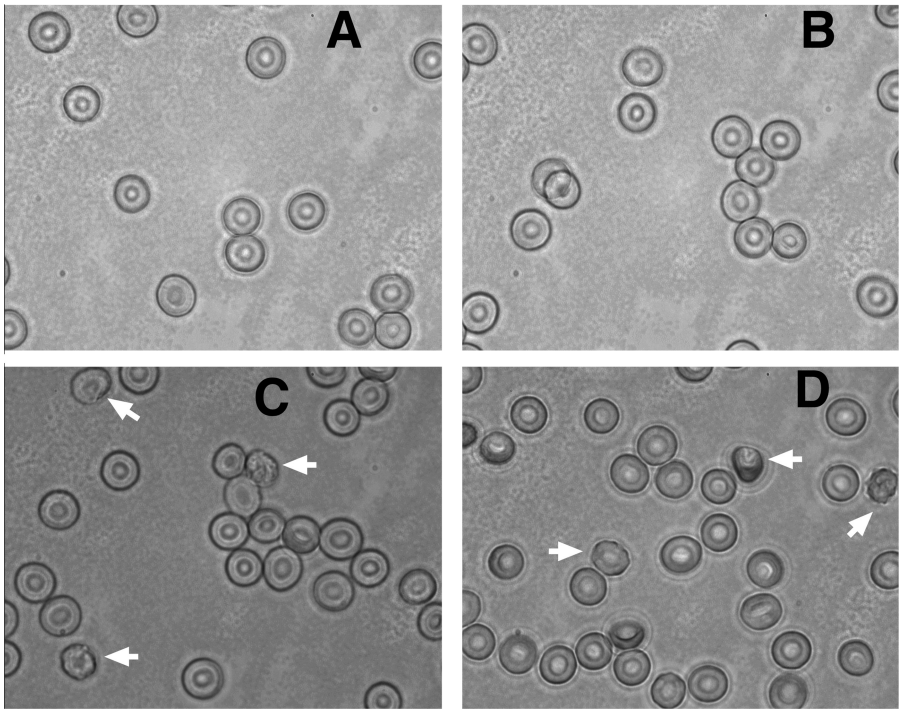

Figure 4. Photomicrographs (100x) of the control (A,B) and PMS-oxidized (C,D) RBC show minimal morphological evidence of physical damage to the oxidized samples. However, a small number of cells in the PMS-treated sample demonstrated some slight morphological evidence (arrows) of damage. These findings, coupled with the automated hematology analyzer data shown in Table I, demonstrate the low sensitivity of these traditional methods to detect damaged RBC. In contrast, clear differences were noted between control and oxidized RBC using the prototype microfluidic device.

In aggregate, the overall mean for the normal and mildly oxidized RBC were 20.13 $\pm$ 1.47 and 27.51 $\pm$ 3.64 pN/μm, respectively, demonstrating that PMS-oxidation of the RBC significantly ($P < 0.0001$) decreased the ability of RBC to deform through the microcapillary channel. While some overlap between the normal and mildly oxidized population distribution was observed, a clear separation of the mean deformability value and distribution profiles of the normal and oxidized RBC was readily detected using the 2–2.5 μm funnel-shaped constriction of the prototype microfluidic plate (Fig. 3). The extensive pressure differential between the "tails" of the normal RBC relative to the oxidized cells allows for an easy diagnostic end point for "abnormal" cells. Furthermore, the microfluidic plate proved more efficient than an ADVIA Hematology Analyzer in identifying abnormal (i.e., oxidized) samples from the normal samples. As shown in Table I, normal and oxidized RBC demonstrated virtually identical parameters with no discernable evidence of damage to the oxidized RBC. Microscopic analysis of the untreated and 50 μM PMS treated RBC demonstrated only minor differences between the populations. As shown in Fig. 4, control RBC (Panels A and B) exhibit normal biconcave structure with clearly delineated (i.e., smooth) edges. In contrast, a small subset of the oxidized RBC (Panels C and D) demonstrate an abnormal morphology though the noted changes were quite modest in nature reflecting the mild oxidative challenge. Hence, in contrast to the microfluidic analysis (Figs. 2-3) both automated hematological analysis and RBC morphological studies suggested that the control and oxidant treated RBC should exhibit similar biological properties.

While *in vivo* analysis of human RBC could not be readily done, a murine transfusion model was employed to determine if the detectable changes in microfluidic deformability yielded a differential biological outcome. As demonstrated in Fig. 5A, murine RBC oxidized by 50 μM PMS exhibited premature clearance despite normal morphology and CBC parameters. Importantly this loss of *in vivo* viability did correlate with the observed changes in microfluidic deformability (Fig. 5B). For comparison purposes, the effects of PMS-treatment of murine cells were compared to the effects of unpaired purified human alpha-hemoglobin chains (model ß thalassemic cells) on murine circulation. Previous studies have also suggested that the mild oxidation induced by 50 μM PMS resembles RBC oxidation levels observed in HbS and ß Thalassemic RBC suggesting that microfluidic analysis of donor samples could be used to screen for hemoglobinopathies or other RBC abnormalities characterized, at least in part, by decreased deformability.

To further assess the utility of the microfluidic device to act as a screening device, deformability of RBC obtained from finger pricks (versus venous draws used in the above studies) from 15 donors was assessed. As shown in Fig. 6A, finger prick sampling yielded findings similar to that of venous blood draws with a mean of 20.49 $\pm$ 1.67 pN/μm (versus 20.13 $\pm$ 1.47 pN/μm for venous blood draws; mean and standard deviation of 15 individuals). While variability was noted between individual donors (Fig. 6B), it is important to note that none of the 'normal' (i.e., unscreened for any hematological abnormalities) individuals exhibited a mean deformability value (in pN/μm) similar to the PMS-oxidized RBC. This data demonstrated the potential utility of the microfluidic device in screening for RBC abnormalities in the general population that would not be detected by other measures such as automated hematology analyzers (Table I) or morphological analysis (Fig. 4).

Discussion

While the most commonly perceived functions of the RBC are to deliver O_2 and remove CO_2, these biologically essential tasks could not be accomplished absent the unique deformability of the intact erythrocyte [3,11–13,16]. As shown in Fig. 7A, the relatively large human and murine

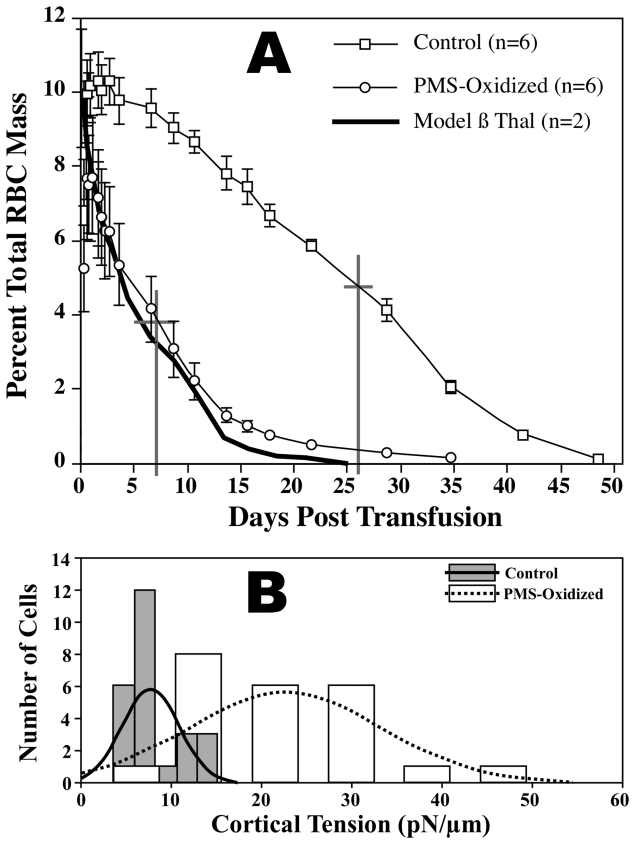

Figure 5. Microfluidic detection of poorly deformable cells correlated with poor *in vivo* survival in a murine transfusion model. Panel A: As shown the PMS-treated RBC demonstrated half-life (denoted by gray crosses) of 7 days in the peripheral murine circulation. This is in stark contrast to the 26 day half-life for normal mouse RBC. RBC survival was measured using membrane labeling of cells with PKH-26. Shown is the percent total RBC mass that was PKH-26 labeled. The PMS dosage used in this study results in very mild oxidation of mouse hemoglobin (~30% methemoglobin). Previous studies by our laboratory and others have demonstrated that this dosage of PMS on human RBC induces comparable iron release to that seen in thalassemic and sickle RBC. For comparison purposes, the survival curve for model ß-thalassemic murine RBC is also shown. Model ß Thalassemic murine RBC were made by the entrapment of purified human α-hemoglobin chains within normal mouse RBC. Panel B: Oxidative injury results in a significant loss of cellular deformability as noted by the increased cortical tension.

RBC must be capable of deforming through capillaries and splenic pores ranging in size from ~2.5 to 0.5 μm. Depending on the diameter of the pore, this deformation process includes both elongation and folding events. Indeed, pharmacologic agents or hemoglobin, cytoskeletal, metabolic or lipid abnormalities that impair the deformability of the RBC will give rise to the premature clearance of the cell and, potentially, anemia. Because of the crucial biological importance of RBC deformability, numerous methodologies have been devised to measure both cellular and membrane deformability [3,26–33]. These approaches include ektacytometry, micropore transit analyses, and micropipette aspiration. However, all these approaches require expensive instrumentation, are time-consuming and are unsuitable for high-throughput use in the blood bank, clinic or in the field [33].

Microfluidic deformability analyses may represent a rapid and low cost means of evaluating RBC deformability in red cell products (fresh and stored). Moreover, these easy to use devices may also be useful in screening individuals in remote locations for undiagnosed RBC abnormalities (e.g., SCD and thalassemias) or diseases (e.g., malaria infection). While the design used in the current study (Fig. 1) was a low throughput, individually molded and manually operated device the primary principals (channel geometry and pressure range) are easily applied to an automated, high throughput, microfluidic device that is fully self-contained [43,44]. Of biological interest, this proof-of-concept microfluidic device clearly demonstrated a reproducible range for different human donors (Figs. 2-3, and 6) as well as limited variability within the same donor over time (days to weeks). More importantly, mildly oxidized RBC could be efficiently detected by a right-shift and widening of the RBC distribution curve (Figs. 2-3).

However, as noted, the mean pore size of the prototype microfluidic device ranged from 2.0 to 2.5 μm. The fluctuation in pore size could introduce some variation in the pressure required for pore transit. Indeed, the measured pressures (mean ± SD) of normal washed RBC for Donors A–D over the 14–21 days sampling timepoints are 10.35 ± 0.90, 11.09 ± 0.87, 11.9 ± 1.55, and 11.58 ± 1.59 Pa. The variation in values could arise either due to biological variances or due to the effect of small differences in the pore size of the individual microfluidic devices. For example, for Donor A sampled at Days 0, 7 and 21 the measured pore sizes were, respectively, 2.35, 2.17, and 2.43 μm and the measured pressures were 9.69, 11.35, 10.13 Pa. Similar trend has been observed for Donor B, C, and D, where bigger pore sizes lead to smaller measured pressure. Typically, the pore size used to determine threshold pressure range from 2.1 to 2.5 μm. Therefore, cortical tension was used as a relative measurement of deformability of red cell to adjust for the funnel geometry (size) variation. The cortical tension values of normal red cells for Donors A–D were 19.83 ± 0.95, 19.90 ± 1.04, 21.40 ± 1.61, and 19.37 ± 1.94 pN/μm, respectively. These results show that the coefficient of variance (CV) value (standard deviation/average for each donor) for cortical tension is on average 7% compared with 11% of raw pressure measurements. The reduced CV indicates the model is effective for compensating for the variation in cell size and in particularly, pore size. Once an improved manufacturing technique is developed to ensure consistent and stable funnel geometry, pressure alone may be sufficient to indicate RBC deformability.

Of biological and clinical importance, the observed right-shift in the deformability profile of the oxidized murine RBC correlated with accelerated circulatory clearance in a murine transfusion model (Fig. 5). Through extensive *in vivo* testing, it may be possible using the microfluidic device to determine a threshold (Fig. 7B; *v*) at which point circulatory clearance will likely to occur. Worth noting was the observation that the PMS-treated cells showed minimal differences from control RBC when analyzed on an automated hematology analyzer (Table I) and only minor evidence of morphological abnormalities (Fig. 4) when analyzed within an hour after treatment. However, over time the damage becomes more apparent. Indeed, the oxidant and challenge dosage (50 μM PMS) used in this study was specifically chosen as previous studies have demonstrated that the oxidant treated RBC exhibited similar characteristics to sickle and thalassemic cells [15,17,24]. In support of this finding, the PMS-treated murine cells demonstrated very similar *in vivo* circulation to that of model ß thalassemia murine RBC [3,17,49].

Microfluidic deformability testing can also be done on very small blood samples. As shown in this study, the deformability profiles of samples obtained via a venous blood draw correlated exceptionally well with a blood droplet collected via a finger prick (Figs. 2-3, and 6). Consequent to this finding, it would be possible to use such a device in remote locations to screen populations for hematological analysis prior to more technologically

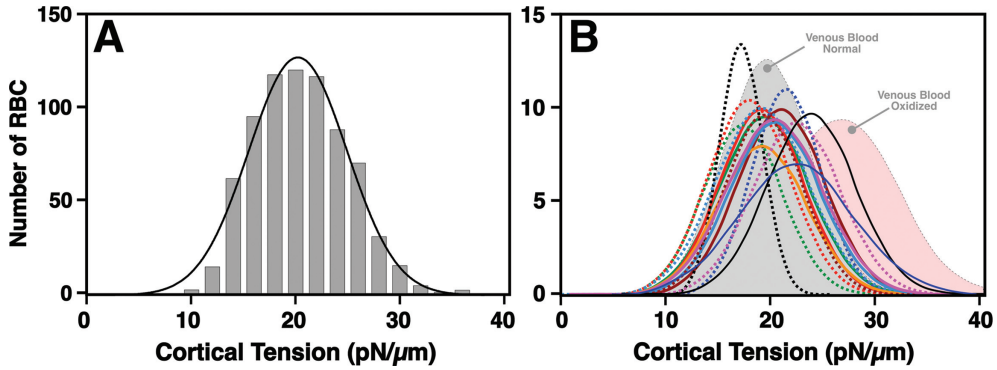

Figure 6. Microfluidic deformability assays of blood obtained via finger prick correlate well with venous blood findings. Panel A: Shown is the mean finger-prick deformability distribution curve derived from 15 individual donors. Panel B: Shown are the individual distribution curves for the 15 donors overlaid on the venous blood draw findings (see Fig. 3) for normal (grey shaded distribution curve) and oxidized (pink shaded distribution curve) RBC. Deformability profiles were collected using 15 individual (disposable) microfluidic devices over the course of approximately 3 weeks.

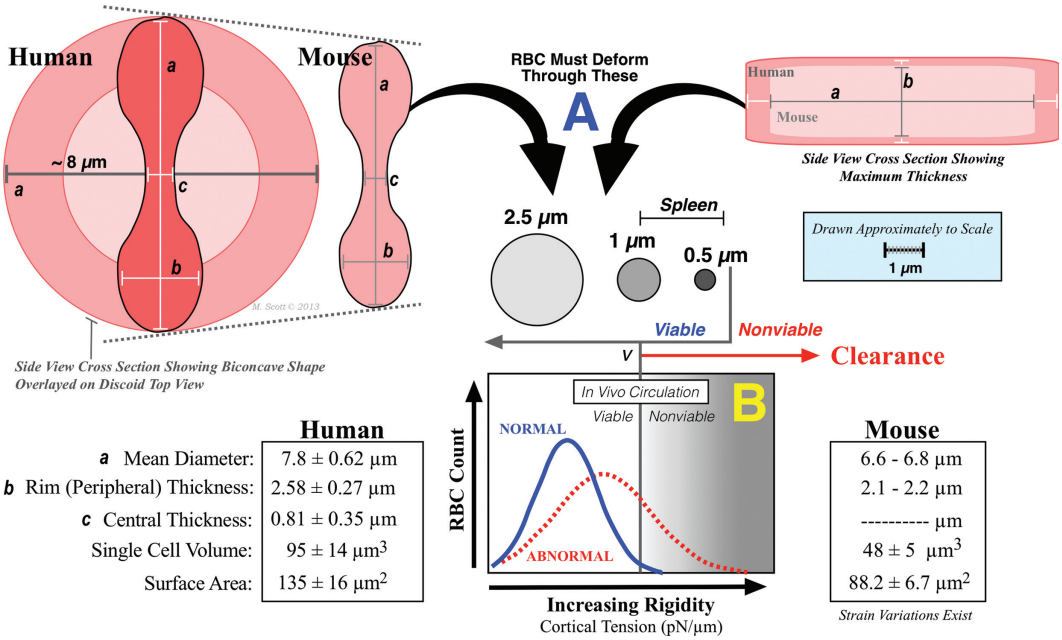

Figure 7. Schematic representation of human and murine RBC and the capillary and interendothelial splenic pore diameters (Panel A). The mean diameter (*a*), rim thickness (*b*) and central thickness (*c*) for human and murine cells are noted. All objects are drawn approximately to scale as noted. Panel B: Abnormal RBC (dashed line) is increasingly rigid as determined by increased cortical tension (pN/μm). As demonstrated in our murine transfusion study, a large percentage of these cells are nonviable *in vivo* and consequently cleared from circulation. Line *(v)* represents a microfluidic detection threshold at which point circulatory clearance is likely to occur via the spleen or capillary entrapment as well as by other mechanisms. This threshold can be experimentally determined and would be of clinical value; especially with regards to stored donor RBC.

discriminating (and expensive) assays. Ongoing work is underway to determine if the microfluidic device could be used to further discriminate between specific hematologic abnormalities (e.g. SCD versus ß-Thalassemia). This could be accomplished via changes of micropore geometry and/or deoxygenation of the samples within the microfluidic device. Importantly, the proposed microfluidic device is a screening not a definitive diagnostic device. By establishing a standard deformability distribution profile from hematologically normal individuals, blood samples exhibiting either a *left* of *right* shift from the expected distribution curve would then be further tested to define specific hematological defects.

The portability and low cost of a microfluidic deformability assessment device holds great promise relative to traditional deformability assays (e.g., Ektacytometry). The current study demonstrated that the manually operated, low throughput prototype device reliably detected significant differences between normal and abnormal red cells via cortical tension analysis. However, for practical use, significant improvements will be needed. Our ongoing work on the development of an automated, high throughput microfluidic device will allow for the efficient (and low cost) screening of large numbers of individuals in a standardized fashion.

While additional research and development is necessary to further define and validate a self-contained, high throughput microfluidic device, this study demonstrates the reproducibility and potential utility of this approach to measuring RBC deformability. Moreover, the microfluidic deformability device allows for large-scale sampling of population via a simple finger prick; an approach that would prove highly useful in screening remote populations for hematological abnormalities. Of further clinical

interest, current studies within our laboratory are examining the utility of microfluidic deformability in assessing the RBC storage lesion [50–53]. The findings of these studies may prove useful in establish "*good*" versus "*bad*" stored RBC prior to transfusion of the blood product into recipients. In summary, microfluidic analysis of RBC deformability may have significant utility in screening for hematologic abnormalities and in evaluating the biological viability of fresh and stored donor RBC products thus yielding safer and more effective transfusions to at risk individuals.

Acknowledgments

The authors would like to thank Ms. Wendy Toyofuku and Dr. Yevgeniya Le for their laboratory guidance and Mr. Yen-Po Liu for his assistance in the fabrication of the microfluidic devices. The views expressed herein do not necessarily represent the view of the federal government of Canada. We thank the Canada Foundation for Innovation and the Michael Smith Foundation for Health Research for infrastructure funding at the University of British Columbia Centre for Blood Research.

References

1. Chen LT, Weiss L. The role of the sinus wall in the passage of erythrocytes through the spleen. Blood 1973;41:529–537.
2. Weiss L, Tavassoli M. Anatomical hazards to the passage of erythrocytes through the spleen. Sem Hematol 1970;7:372–380.
3. Scott MD, Rouyer-Fessard P, Ba MS, et al. Alpha- and beta-haemoglobin chain induced changes in normal erythrocyte deformability: Comparison to beta thalassaemia intermedia and Hb H disease. Br J Haematol 1992;80: 519–526.
4. Diez-Silva M, Dao M, Han J, et al. Shape and biomechanical characteristics of human red blood cells in health and disease. MRS Bull 2010;35:382–388.
5. Barabino GA, Platt MO, Kaul DK. Sickle cell biomechanics. Annu Rev Biomed Eng 2010;12:345–367.
6. Chien S, Usami S, Bertles JF. Abnormal rheology of oxygenated blood in sickle cell anemia. J Clin Invest 1970;49:623–634.
7. Chien S. Red cell deformability and its relevance to blood flow. Annu Rev Physiol 1987;49:177–192.
8. Reinhart WH, Chien S. Roles of cell geometry and cellular viscosity in red cell passage through narrow pores. Am J Physiol 1985;248:C473–C479.
9. Sung KL, Chien S. Influence of temperature on rheology of human erythrocytes. Chin J Physiol 1992;35:81–94.
10. Baskurt OK. In vivo correlates of altered blood rheology. Biorheology 2008;45: 629–638.
11. Weed RI, LaCelle PL, Merrill EW. Metabolic dependence of red cell deformability. J Clin Invest 1969;48:795–809.
12. Weed RI. The importance of erythrocyte deformability. Am J Med 1970;49: 147–150.
13. Weed RI. Mechanical properties of the erythrocyte as determinants of red cell birth and death. Clin Sci 1972;42:8P.
14. Goldstein DB. The effects of drugs on membrane fluidity. Annu Rev Pharmacol Toxicol 1984;24:43–64.
15. Hebbel RP, Leung A, Mohandas N. Oxidation-induced changes in microrheologic properties of the red blood cell membrane. Blood 1990;76: 1015–1020.
16. Vaya A, Iborra J, Falco C, et al. Rheological behaviour of red blood cells in beta and deltabeta thalassemia trait. Clin Hemorheol Microcirc 2003;28: 71–78.
17. Scott MD, van den Berg JJ, Repka T, et al. Effect of excess alpha-hemoglobin chains on cellular and membrane oxidation in model beta-thalassemic erythrocytes. J Clin Invest 1993;91:1706–1712.
18. Stuart MJ, Nagel RL. Sickle-cell disease. Lancet 2004;364:1343–1360.
19. Chasis JA, Schrier SL. Membrane deformability and the capacity for shape change in the erythrocyte. Blood 1989;74:2562–2568.
20. Rachmilewitz EA, Shinar E, Shalev O, et al. Erythrocyte membrane alterations in beta-thalassaemia. Clin Haematol 1985;14:163–182.
21. Schrier SL, Rachmilewitz E, Mohandas N. Cellular and membrane properties of alpha and beta thalassemic erythrocytes are different: Implication for differences in clinical manifestations. Blood 1989;74:2194–2202.
22. Schrier SL. Thalassemia: Pathophysiology of red cell changes. Annu Rev Med 1994;45:211–218.
23. Shinar E, Shalev O, Rachmilewitz EA, et al. Erythrocyte membrane skeleton abnormalities in severe beta-thalassemia. Blood 1987;70:158–164.
24. Scott MD, Eaton JW, Kuypers FA, et al. Enhancement of erythrocyte superoxide dismutase activity: Effects on cellular oxidant defense. Blood 1989;74: 2542–2549.
25. Scott MD. Intraerythrocytic iron chelation: A new therapy for thalassemia. Hematology 2001;6:73–89.
26. Kuypers FA, Scott MD, Schott MA, et al. Use of ektacytometry to determine red cell susceptibility to oxidative stress. J Lab Clin Med 1990;116: 535–545.
27. Bronkhorst PJ, Streekstra GJ, Grimbergen J, et al. A new method to study shape recovery of red blood cells using multiple optical trapping. Biophys J 1995;69:1666–1673.
28. Baskurt OK. Deformability of red blood cells from different species studied by resistive pulse shape analysis technique. Biorheology 1996;33:169–179.
29. Kuypers FA, Schott MA, Scott MD. Phospholipid composition and organization in model beta-thalassemic erythrocytes. Am J Hematol 1996;51:45–54.
30. Murad KL, Mahany KL, Brugnara C, et al. Structural and functional consequences of antigenic modulation of red blood cells with methoxypoly(ethylene glycol). Blood 1999;93:2121–2127.
31. Dobbe JG, Hardeman MR, Streekstra GJ, et al. Analyzing red blood cell-deformability distributions. Blood Cells Mol Dis 2002;28:373–384.
32. Streekstra GJ, Dobbe JG, Hoekstra AG. Quantification of the fraction poorly deformable red blood cells using ektacytometry. Opt Express 2010;18: 14173–14182.
33. Musielak M. Red blood cell-deformability measurement: Review of techniques. Clin Hemorheol Microcirc 2009;42:47–64.
34. Baskurt OK, Fisher TC, Meiselman HJ. Sensitivity of the cell transit analyzer (CTA) to alterations of red blood cell deformability: Role of cell size-pore size ratio and sample preparation. Clin Hemorheol 1996;16:753–765.
35. Whitesides GM. The origins and the future of microfluidics. Nature 2006;442: 368–373.
36. Bransky A, Korin N, Nemirovski Y, et al. Correlation between erythrocytes deformability and size: A study using a microchannel based cell analyzer. Microvasc Res 2007;73:7–13.
37. Forsyth AM, Wan J, Ristenpart WD, et al. The dynamic behavior of chemically "stiffened" red blood cells in microchannel flows. Microvasc Res 2010;80: 37–43.
38. Martin JD, Marhefka JN, Migler KB, et al. Interfacial rheology through microfluidics. Adv Mater 2011;23:426–432.
39. Patel KV, Mohanty JG, Kanapuru B, et al. Association of the red cell distribution width with red blood cell deformability. Adv Exp Med Biol 2013;765: 211–216.
40. Shevkoplyas SS, Yoshida T, Gifford SC, et al. Direct measurement of the impact of impaired erythrocyte deformability on microvascular network perfusion in a microfluidic device. Lab Chip 2006;6:914–920.
41. Ye T, Li H, Lam KY. Modeling and simulation of microfluid effects on deformation behavior of a red blood cell in a capillary. Microvasc Res 2010;80: 453–463.
42. Guo Q, Reiling SJ, Rohrbach P, et al. Microfluidic biomechanical assay for red blood cells parasitized by Plasmodium falciparum. Lab Chip 2012;12: 1143–1150.
43. Guo Q, McFaul SM, Ma H. Deterministic microfluidic ratchet based on the deformation of individual cells. Phys Rev E Stat Nonlin Soft Matter Phys 2011; 83:051910.
44. Guo Q, Park S, Ma H. Microfluidic micropipette aspiration for measuring the deformability of single cells. Lab Chip 2012;12:2687–2695.
45. Schlegel RA, Lumley-Sapanski K, Williamson P. Single cell analysis of factors increasing the survival of resealed erythrocytes in the circulation of mice. Adv Exp Med Biol 1992;326:133–138.
46. Scott MD, Murad KL, Koumpouras F, et al. Chemical camouflage of antigenic determinants: Stealth erythrocytes. Proc Natl Acad Sci U S A 1997;94: 7566–7571.
47. Wang D, Kyluik DL, Murad KL, et al. Polymer-mediated immunocamouflage of red blood cells: Effects of polymer size on antigenic and immunogenic recognition of allogeneic donor blood cells. Sci China Life Sci 2011;54: 589–598.
48. Scott MD, Kuypers FA, Butikofer P, et al. Effect of osmotic lysis and resealing on red cell structure and function. J Lab Clin Med 1990;115: 470–480.
49. Scott MD, Rouyer-Fessard P, Lubin BH, et al. Entrapment of purified alpha-hemoglobin chains in normal erythrocytes. A model for beta thalassemia. J Biol Chem 1990;265:17953–17959.
50. Wolfe LC, Byrne AM, Lux SE. Molecular defect in the membrane skeleton of blood bank-stored red cells. J Clin Invest 1986;78:1681–1686.
51. Wolfe LC. Oxidative injuries to the red cell membrane during conventional blood preservation. Sem Hematol 1989;26:307–312.
52. Klein HG, Spahn DR, Carson JL. Red blood cell transfusion in clinical practice. Lancet 2007;370:415–426.
53. Anniss AM, Glenister KM, Killian JJ, et al. Proteomic analysis of supernatants of stored red blood cell products. Transfusion 2005;45:1426–1433.